journal

homepage:

www.elsevier.com/locate/margo

High-resolution 3D seismic exhibits new insights into the middle-late Pleistocene stratigraphic evolution and sedimentary processes of the Bear Island trough mouth fan.

Malin Waage[a,*], Stefan Bünz[a] , Reidulv Bøe[b] , Jurgen Mienert[a]

*Corresponding author, e-mail address: malin.waage@uit.no (M. Waage)

[a] Centre for Arctic Gas Hydrate, Environment and Climate (CAGE), Department of Geosciences, UiT The Arctic University of Norway, 9037 Tromsø, Norway

[b]Geological Survey of Norway, P.O. Box 6315, Torgarden, 7491 Trondheim, Norway

Abstract

Arctic Ocean trough mouth fans (TMFs) represent a valuable archive of glacial-interglacial sedimentary processes that are especially important when reconstructing pre-Weichselian glaciations that may lack distinct imprints on the shelves. In 2011, we acquired the first high-resolution 3D seismic cube (~3 m vertical and 6 m horizontal resolution) on the continental slope of the SW Barents Sea by use of a P-Cable 3D system, to study in detail the seismic stratigraphy and glacial depositional history of the Bear Island Trough Mouth Fan. This technology provides data with a resolution that, for the first time on the western Barents Sea slope, enables detailed mapping of deposits of different glacial cycles. The dataset provides entire spatially coverage, allowing us to reconcile multiple generations of glacigenic deposits and channel systems. High-resolution 3D seismic data is crucial to describe buried channels, glacial units, as well as low relief landforms such as sediment waves accurately. The 30 km2 seismic cube is located at the southern flank of the Bear Island TMF at water depths from 592 to 660 m where sandwaves dominate the present seafloor. The data covers the glacially derived stratigraphy in the uppermost ~700 m below the seafloor. We establish a robust stratigraphic framework by interpreting seismic reflectors along 2D tie-in lines to previously well-constrained seismic and well data. We find that our data provide a record of progradation of glacigenic debris flows (GDFs) since MIS 12 (0.5 Ma) to present. Horizon slices reveal

a range of gullies and channels at different depths overlying the GDFs. We describe the paleoenvironment and sedimentary processes throughout this time-span (that covers seven glacial cycles) and discuss the impact of the Barents Sea Ice Sheet waxing and waning on erosion, sedimentation, and deposition along the continental slope. Abundant buried gullies were hitherto unknown at the Bear Island TMF, with previous work describing this succession as a debris-flow dominated unit where meltwater-related features are lacking, and interpreting this to represent low average temperatures. By use of the relatively small high-resolution 3D seismic dataset, we provide new evidence for the presence of gullies and channels indicating that periods of ice sheet melting and meltwater runoff existed throughout the middle-late Pleistocene succession. The work offers new insight into the stratigraphic evolution of a continental margin dominated by GDFs and demonstrates the value of high-resolution seismic, such as the P-Cable system, in resolving important details of paleo-slope-environments.

1. Introduction

The Barents Sea is a shallow epicontinental sea with an average water depth of 280 m. Towards the North Atlantic Ocean, the western shelf edge can be up to 400 m deep extending from northern Norway to Svalbard (Fig. 1). Similar to other formerly glaciated passive continental margins, advance and retreat of ice sheets has controlled erosion, transport, and deposition of sediments from the shelf to the continental slope (Dowdeswell et al., 2016). Accordingly, shallow banks and deep troughs of glacial origin sculpture the Barents Sea continental shelf (Jakobsson et al., 2014).

The Bear Island Trough is the largest erosional feature, covering an area of about 100,000 km2 with a trough length of > 100 km (Fig. 1) (Laberg and Vorren, 1995). Over the last 5 Ma, glaciations have been responsible for ~100 km westward advances of the Barents Sea margin (Vorren et al., 1989). Up to 2 km of predominantly glacially eroded sediments have been deposited on the slope, building the Bear Island Trough Mouth Fan (Bear Island TMF) during the Pleistocene glaciations(Vorren et al., 1989) (Figs. 1 and 2).

A variety of erosional landforms including chutes, channels, gullies, debris flows and ploughmarks, as well as intermittent contourite deposits reflect the slope-depositional environment of the TMF (Vorren et al., 1989; Laberg et al., 2012; Buhl-Mortensen et al., 2015; King et al., 2014; Bøe et al., 2015; Bellec et al., 2016). Similar to other TMF, the Bear Island TMF typically comprises glaciogenic, muddy debris flows enclosed between thin (< 10 m) units of well-sorted hemipelagic/glaciomarine mud (Vorren et al., 1989; Sættem et al., 1992). The debris flows

65 are suggested to have been deposited when the ice sheet was close to or at the shelf edge
66 (Vorren et al., 1989, Sættem et al., 1992). Seismic data commonly show characteristics of debris
67 flow units as discontinuous, undulating to mounded reflectors alternating with semitransparent
68 intervals (Vorren et al., 1989; Sættem et al., 1992; Vorren and Laberg, 1997; Laberg and Vorren,
69 1996; Sættem et al., 1994).

70 When the shelf was deglaciated during interglacial periods, sediment supply from the shelf to
71 the Barents Sea continental slope decreased significantly, and the depositional environment was
72 mainly controlled by downslope transport driven by submarine slides or alongslope transport by
73 ocean currents (Bryn et al., 2005). At present, the northward flowing North Atlantic Current has
74 velocities of 0.2 to ~1 m/s along the upper slope (~500 to 800 m water depth) between ~71°N
75 and 72°N (Poulain et al., 1996; Bøe et al., 2015; Skarðhamar et al., 2015). This current, together
76 with internal waves, cause today's formation and migration of characteristic sandwaves on the
77 seafloor (Kenyon, 1986; King et al., 2014).

78 In an extensive seismo-stratigraphic study following regional reflectors, Faleide et al. (1996)
79 divided the Plio-Pleistocene succession (2.7 Ma to present) along the western Barents Sea slope
80 into three regional seismo-stratigraphic units: GI, GII and GIII (Fig. 2). Combined with
81 paleomagnetic, biostratigraphic and Sr-isotope analysis of borehole data from ODP site 986, Butt
82 et al. (2000) revised a sparse existing chronology and suggested three phases of glaciation during
83 this period. The third and last glacial phase started ~0.5 million years ago (Ma), and is
84 characterized by major erosional and extensive ice-sheet drainage events towards the shelf edge
85 of the western Barents Sea. The period is described as a cold phase when ice masses began to
86 advance and retreat across the entire continental shelf to their maximum positions at the shelf
87 edge (Solheim et al., 1996; Butt et al., 2000).

88 More detailed seismo-stratigraphic studies of the W Barents Sea continental slope have
89 divided the GIII unit into 4–8 subunits. Close to the study area of this work, Sættem et al. (1992)
90 used magneto-stratigraphy and amino acid dating from key seismic horizon depths indicating
91 maximum ages (with an uncertainty of one standard deviation) and identified four major glacial
92 advances between 440 and 130 ka BP. Subsequently, Svendsen et al. (2004) identified another
93 three glacialinterglacial cycles between 130 ka BP and the present, based on satellite data, aerial
94 photographs, geological field data from Russia and Siberia and marine seismic- and sediment
95 core data.

96 There are a few studies that have used 3D seismic for investigating the Plio-Pleistocene
97 succession along the Western Barents Sea margin (Larsen et al., 2003; Andreassen et al., 2007;

Laberg et al., 2010). Andreassen et al. (2007) showed evidence for fast-flowing ice streams on the outer shelf during earlier glaciations, while Laberg et al. (2010) investigated paleo-slope environments and depositional processes along the Bear Island TMF slope. All these studies used the 3D industry seismic data, but without high enough resolution or lateral extent to resolve the entire regional GIII unit.

The presence of extended fields of seafloor sandwaves crossing the upper slope of the Bear Island TMF led to the selection of the specific site to acquire the high-resolution P-Cable 3D seismic cube (Fig. 1). A high-resolution seismic stratigraphy enables deciphering of diagnostic features such as sediment waves, channels, gullies and debris flows that dominate high-latitude continental slopes in either glacial or interglacial times. Identification of sandwave activities during previous interglacials can provide valuable information on the reorganization of currents along the Norwegian continental margin after an ice age, and thus, the extent of along-slope transport of sediments at continental margins.

Nevertheless, this is the first time the glacial stratigraphy of SW Barents Sea slope is described in such detail to resolve glacial-interglacial cycles and thus with better confidence detect paleo-seafloors and individual debris-flow successions. The data is used together with results from previously published papers and regional 2D seismic lines to investigate in detail the seismic stratigraphy and glacial depositional history of the fan during the Plio-Pleistocene. The results provide new insight into the stratigraphic evolution of a continental margin dominated by GDFs.

2. Methods

2.1. P-Cable 3D seismic processing, interpretation, and visualization

The 3D seismic dataset "SandWaveNorth_3D" was acquired in July 2011 using the high-resolution P-Cable 3D seismic system (Petersen et al., 2010) onboard RV Jan Mayen (now RV Helmer Hansen) (Location in Fig. 1). One mini-GI airgun with a chamber volume of 15/15 in.3 and a shooting rated of 4 s provided the seismic energy for sub-seabed penetrations up to 700 m below the seafloor. Data processing was performed using RadexPro (2011) software, developed for the P-Cable system (Petersen et al., 2010). In addition to a standard processing workflow using a bin size of 6.25 × 6.25 m, we performed tidal and static corrections and a 3D Stolt-migration with a 1500 m/s seismic velocity (see Petersen et al. (2010) for further details on the processing). The seismic has a dominant frequency of 170 Hz between the seafloor to the depth

where the seismic energy becomes too low for identifying seismic reflections. While the average horizontal resolution is comparable with the bin-size of 6.25 m, we calculated an average vertical resolution of 3 m using the Rayleigh criterion (Culick, 1987). In-line acquisition noise appears as slightly elevated, and higheramplitude bands parallel to the in-line direction. Throughout the 3D seismic dataset, a weak seismic amplitude pattern mirrors the amplitude anomalies on the seafloor caused by sandwaves.

We performed 3D seismic analysis, visualization, and interpretation using the seismic interpretation software Petrel. While investigating the subsurface we applied and examined the data with various attributes, as curvature maps, sediment thickness maps, and root mean square (RMS) amplitude maps (Brown et al., 1996).

Based on an average sediment velocity of 1970 m/s, extracted from Fiedler and Faleide (1996) for unit GIII, and assuming that sediment compaction increases slightly with depth, we used a 1600–2100 m/s linear increase in sediment velocity between the seafloor and the base of unit GIII to convert the seismic data from two-way travel time (TWT [ms]) to depth (m) (Christensen and Mooney, 1995).

2.2. Seismic correlation and age control

We traced the most prominent, regional reflectors within the middle-late Pleistocene unit (GIII unit) from 2D seismic data to our 3D P-Cable seismic cube (Vorren et al., 1990; Sættem et al., 1992; Laberg et al., 2012; Faleide et al., 1996; Ryseth et al., 2003; Larsen et al., 2003). In Fig. 2, we show the correlation from the nearby Sørvestagneset 3D area (location in Fig. 1) (Larsen et al., 2003; Andreassen et al., 2007) and our 3D area via 2D seismic line NH9702 and NH8401. Larsen et al. (2003) divided the GIII stratigraphy into 4 units (E-H), and these units have we correlated to our study site. Another study we correlate to is Sættem et al. (1992), who used magneto-stratigraphy and amino acid dating from key seismic horizon depths indicating maximum ages based on borehole data and high-resolution 2D seismic data of the outer Bear Island slope. Seismo-stratigraphic correlation has also been done between the study area of Sættem et al. (1992) and the Sørvestagneset 3D area (Larsen et al., 2003).

The well-defined R1 reflector represents the base of the GIII succession (Vorren et al., 1990, Sættem et al., 1992, Laberg et al., 2012, Faleide et al., 1996, Ryseth et al., 2003, Larsen et al., 2003). In the study area, the base of the middle-Pleistocene succession (R1) appears at 600–800 m below the seabed (< 1600 TWT) (Fig. 2).

We base our interpretation of glacial cycles in the seismic stratigraphy on the identification of pervasive, continuous reflectors with erosional characteristics (interglacials/interstadials) separating units with typical seismic signatures of debris flows (glaciations/stadials). When correlating the different units to the time-line of past glacial cycles, we make two assumptions; (1) we have resolved glacial-interglacial cycles and (2) the stratigraphy shows deposition of GDFs at all major glaciations since MIS 12 (suggested start of deposition of the middle-late Pleistocene succession). Based on these assumptions, we used global temperature and inferred ice thickness data from oxygen isotope proxy and marine isotope stages (MIS) from the EPICA Dome C ice cores in Antarctica for the correlation. We further discuss and compare our results with the work of Sættem et al. (1992) and Larsen et al. (2003) with regard to unit and age classification.

3. Seismic horizons and units

We divide the middle to late Pleistocene succession into 6 seismic units (U1–U6 from bottom to top) separated by 6 horizons (R1 and H1- H6 also from bottom to top) (Figs. 3 and 4). The horizons can be traced along conformable reflectors of varying style and intensity which are all continuous and of high amplitude reflection (Fig. 4). Most of the horizons have channel features orientated in SSW-NNE to WSW-ENE direction down the slope (Fig. 4). The units (U1–U6) are typically 50 to 150 m thick and show a chaotic, semi-transparent character. Reflectors below R1 are hardly visible (due to limited seismic penetration) and appear to be chaotic which limits our study to the middle-late Pleistocene (Fig. 4). In the following, the units and their base horizons aredescribed in detail.

3.1. Description of unit U1

Along 2D seismic lines, R1 (base of U1) is continuous, of varying amplitude and often truncates underlying reflectors. An acoustically transparent zone above is characteristic and can be used to trace R1. Where R1 crosses our 3D seismic data (Fig. 2), the overlying transparent zone reaches ~200 m in thickness and is located at ~1100–1300 m below sealevel (mbsl) (Figs. 3, 4). In the 3D data, the reflector also shows a continuous horizon but with undulating character (Fig. 3), truncating underlying reflectors. The dip-orientation of horizon R1 varies from NNW in the south to SSW in the north of the survey.

Unit U1 is a ~180–300 m thick (thickening towards NW) and semitransparent with occasional discontinuous and undulating reflectors. The central part of the unit shows some more continuous reflectors. A regional reflector separating unit E and F of Larsen et al. (2003) can be

traced from Sørvestagneset to our study site. In our 3D data, it strikes through the lowermost part of U1 (Fig. 2) as a weak, semi-continuous reflector. Based on regional 2D seismic data and correlation to Sørvestagneset, we therefore divide the unit in U1a and U1b separated by a semi-continuous seismic horizon.

3.2. Description of unit U2

Horizon H1, separating units U1 and U2, is the lowermost welldefined and continuous low-amplitude reflector in the 3D dataset, occurring between ~817 and 1006 mbsl (Fig. 3). The horizon has a diporientation towards SW and is rather planar with no observable erosional features.

Unit U2 comprises a 41–78 m thick sediment section (Fig. 4). Four semi-continuous, internal reflectors separate 10–40 m thick, semitransparent intervals. The internal reflectors towards the SW tend to be parallel to the basal reflector H1. Intra U2 reflectors are incised by a network of downslope (NE-SW) oriented channels that are 20–30 m wide and ~1–4 m deep (Fig. 3).

3.3. Description of unit U3

The top of unit U2 is defined by horizon H2 at ~946–815 mbsl, which shows a continuous, high amplitude, smoothly undulating reflector that is sub-parallel to H1 (Fig. 3). Its general dip orientation is slightly towards the WSW (Fig. 3). In the southeast, it truncates underlying reflectors, resulting in a thinning of unit U2. A ~150 m wide, and 10–15 m deep incision shows a slightly sinuous pattern (Figs. 3 and 5). The sinuosity (the ratio between the length along the channel axis and the straight line distance between the end points of the channel) however is measured to be 1.04, which defines it as a straight channel (Reimchen et al., 2016). An RMS amplitude attribute map of the horizon highlights three straighter, high-amplitude bands striking SW-NE. The bands lack a measurable elevation along the horizon (Fig. 5).

Unit U3 is a 36–84 m thick and acoustically transparent succession with occasional weak and discontinuous mounded reflectors (Fig. 4). Three V-shaped channels, which are < 200 m wide and 15–25 m deep appear 2–3 km apart (Fig. 5). Their thalwegs/bases correlate with the high amplitude bands along H2 (Fig. 5).

3.4. Description of unit U4

H3 separates unit U3 from the above-lying unit U4 and is a high amplitude, continuous and undulating reflector horizon, occurring between ~884 and 748 mbsl (Figs. 3, 4). The reflector has

an overall dip towards the WSW and is incised by channels that are 1000–1500 m wide, and ~40 m deep (Fig. 3). The channel axes strike at a 15–20° to 4).

Unit U4 is 18–124 m thick and semi-transparent with some weak, discontinuous, mounded reflectors. High amplitude and relatively straight reflectors occasionally appear in the middle of the unit (Fig. 4, x-line).

3.5. Description of unit U5

Horizon H4 defines the base of unit U5 and extends from 685 to 840 mbsl (Fig. 3). The horizon dips towards the SSW-SW and is characterized by seven slightly sinuous, 10–20 m deep and 50–150 m wide, NE-SW trending channels truncating underlying strata (Fig. 3). Anomalously high amplitudes occur at their thalwegs/channels bases (Fig. 4).

Unit U5 is 50–214 m thick and divided into U5a and U5b based on seismic character differences. The lowermost unit U5a is only 10–20 m thick comprising two to three internal, parallel reflectors. U5b has frequent occurrences of sub-horizontal to mounded, truncating semicontinuous reflectors of low to medium amplitude. The upper part alsoshows some chaotic seismic intervals (Fig. 4). V-shaped channels, 10–30 m deep and 20–100 m wide occur throughout the unit at several levels (Fig. 4). The higher amplitudes at their base/thalwegs provide a characteristic acoustic signature, as illustrated by an RMS amplitude map of unit U5 (Fig. 6). From the RMS map, we also identify an NE-SW trend of the channels, similar to the channels along H4. We traced one of the internal reflectors of unit U5b and named it IntraU5 (Fig. 7). The reflector demonstrates two erosional flanks with a well-defined 1–2 km wide channel in between. It cuts through a semi-transparent interval and well into unit U4.

3.6. Description of unit U6 and the seafloor

Horizon H5 is located on top of unit U5 and defines the base of the latest channel-cut followed by infill (unit U6) from 698 to 587 mbsl. The horizon is traced along a continuous but undulating reflector (Fig. 3) that dips towards the SW-SSW. Three V-shaped, 1–2 km wide and 40–60 m deep channels along H5 incise the underlying unit U5. The channels are straight to sinuous and oriented NNE-SSW to NE-SW(Figs. 3, 4).

Unit U6 represents the channel-infill of channels at H5, which can reach up to 62 m in thickness (on average it is 14 m thick within the study area) with an acoustically semi-transparent to chaotic seismic character. However, one to two low amplitude, semi-continuous and undulating reflectors can be traced throughout the unit (Figs. 3, 8). Horizon H5 and the seafloor tend to merge outside of both the sandwave field and the channel areas (Fig. 8).

The seafloor at 592–660 mbsl dips ~4° towards the southwest. The well-developed sandwave field on the seafloor shows sandwaves up to 6.6 m high with wavelengths up to 140 m. They occur continuously along the continental slope between 550 m and 650 m water depth ofthe study area. Sandwaves migrate on top of unit U5, and on top of U6 above gullies (Figs. 1, 3).

3.7. Channel formation and debris flow activity

In general, seismically continuous (regional) reflectors of truncating/erosional character can typically reflect time hiatuses (disconformities) of earlier interglacials or interstadials when deposition ceased for a longer period (Syvitski, 1991). Such paleo-surfaces areindicated to be represented by horizons H1 to H5 (Fig. 4). Some are likely draped by a glacimarine sediment blanket, deposited during interglacial or possibly deglacial periods (Dowdeswell et al., 2016).

The seismic signature (acoustically semi-transparent and chaotic with occasional mounded semi-continuous reflections) that dominate U1 and U3–U6 is typical for debris flow lobes deposited during glaciations (Laberg and Vorren, 1995; Stravers and Powell, 1997; Posamentier and Kolla, 2003; Vorren and Laberg, 1997). GDFs are suggested to represent the primary deposits building up the Bear Island TMF (Laberg and Vorren, 1995; Vorren and Laberg, 1997), as most glaciogenic TMFs around the world (Vorren and Laberg, 1997), and as such we interpret these units to consist of GDFs.

In the very same study area as ours, using chirp sub-bottom profiler data, Bøe et al. (2015) divide our unit U6 in three. Their unit 1 is the uppermost consisting of sandwaves, unit 2 comprises layered glacimarine sediments and unit 3 massive glacial debris flows (indicating shelf-edge glaciations). These observations supports our interpretation of the sediments comprising unit U6 and the other units (U1-U5) that typically show similar seismic signature.

At the horizons between the dominant debris-flow units, and occasionally within the debris flow units, we observe down-slope directed depressions or channels of varying nature (Figs. 3, 4). The channels along H5, that represent the youngest resolvable paleo-seafloor, are the largest within the succession and of similar dimensions to the prominent glacial chutes in the southern part of the SW Barents Sea (BuhlMortensen et al., 2015). These channels are infilled by the debris flow succession of unit U6 (Fig. 8). From the geometry and size of the narrower channels that incise U3, U4 and U5, as well as along H4, we characterize them as slope-gullies, which are widely described on formerly glaciated margins (Kenyon, 1987; Spinelli and Field, 2001; Twichell and Roberts, 1982). Commonly, all gullies show high reflection amplitudes along their thalwegs, which is an indication of erosion or deposition of a different (infilling) material at their base. The observed gullies however typically do not show any evidence of sediment infill apart from the

amplitude change at their base. This therefore suggests that the gullies do not have an infilling different from that which is typical for debris flows. The gullies might therefore represent a general erosive, sediment bypass system, likely associated with dense and erosive meltwater-flow, for example occurring at the end of a glacial period (Sejrup et al., 2005; Twichell and Roberts, 1982; Bellec et al., 2016). This interpretation is consistent with work showing that turbidity currents or cold/dense meltwater discharge caused by ice sheet melting and meltwater runoff are key processes to develop continental-slope gullies (as well as frequent debris-flow activity) (Piper, 1988; Lowe and Anderson, 2003; Gales et al., 2013).

However, there are still large uncertainties when and for how long gullies form during a glacial cycle. Evenly spaced and well-defined gullies are characteristic of stable ice at the shelf edge (forming by subglacial meltwater discharge). For example, off eastern Canada, gullies are absent in areas where advance did not reach the shelf edge (Piper, 2005). On the contrary, weakly defined surfaces that embed gullies within U3-U5, possible reflect alternations of shelf-edge icesheet advance and retreat causing shorter cycles of ice sheet melting and meltwater runoff and thereby less seafloor exposure of these erosional surfaces. Particularly frequent alternations of meltwater discharge (gully formation) and debris-flow deposition are therefore suggested to have taken place during deposition of unit U5b (Fig. 9). Gully formation was a dominant process, punctuating massive sedimentation events.

Channels at the well-defined horizons of H1, H2, and H3 are gentler than along H4 and H5. Typically, gentle channels are observed on the present seafloor in deeper- or gentler slope areas along the margin where the latest glacial down-slope energy/activity was less (Bellec et al., 2016). The channel-gentleness might also be explained by erosion and smoothing by strong along-slope bottom currents in inter-glacial times, considering their location at the upper slope (Vorren et al., 1998).

4. Glacial cycles on the SW Barents Sea continental slope

Glacial-interglacial cycles from the EPICA Dome C temperature-record of ice-ages and ice-sheet thickness matches well with Larsen et al.'s(2003) proposed shelf edge glaciation-curve for the Western Barents Sea Margin over the last 0.5 Ma. This implies that the EPICA Antarctica record of past temperature variations is useful to constrain the age of past ice-sheet advance and retreat in the Barents Sea, where no comparable ice-record exists (Fig. 9).

According to our seismic correlation, the lowermost unit U1a is located directly above the regional reflector R1, leading us to suggest that unit U1a and U1b correspond to the glaciations that occurred during MIS 12 and MIS 10, ~470–430 and 380–340 ka ago, respectively (Fig. 9). The suggested time of deposition and units correlate with Sættem et al.'s (1992) unit B (and C), which they suggest were deposited during two glacial events between ~440 and 330 ka BP.

The paleo-surface of H1 (that defines the base of overlying U2) can be identified as the interglacial period of MIS 9, which we indicate to have been exposed subaerially 340–325 ka ago (Fig. 9). This interglacial period occurred before a prolonged gradual cooling period (325–290 ka ago), when deposition of the semi-flat lying sediments of unit U2 occurred. The unit has several internal, semi-continuous horizons with characteristics similar to H1, suggesting that the shelf-ice sheet was located further away from the shelf edge over a long period.

The thickness and reflection patterns of units U3 and U4, dominated by GDFs, clearly reflect depositional environments linked to maximum glaciations on the Barents Sea shelf. The next glaciations, from iceproxy records, occurred at ~290–250 BP (correlating to MIS 8) and at ~225–135 ka BP (correlating to MIS 6) (Fig. 9). Hence, we suggest that units U3 and U4 were deposited during maximum glaciations of MIS 8 and 6, respectively. The semi-continuous horizon of high-amplitude within U4 might thus have formed during the interstadial period around 200 ka BP, when ice did not reach the shelf edge over a period of ~30 ka years. We find units U3 and U2 to correlate with Sættem et al.'s (1992) unit D1, and our unit U4 to Sættem et al.'s (1992) unit D2 and Larsen et al.'s (2003) unit G. Following Sættem et al.'s (1992) age estimates, unit C-D2 where deposited between 330 and 130 ka BP, which correlate well with our interpretations.

No stratified unit indicating glacimarine or marine sediments occurs between these units, which might be explained by the short interglacial time span (only ~10 ka) that separate the units, thus giving little time to accumulate marine sediments (Fig. 9). A relatively warm, longer lasting interglacial occurred at MIS 5 at ~130 to 110 ka BP which we correlate to the < 20 m stratified unit U5a. We propose that the unit comprises marine, glaciomarine or hemipelagic mud. At this depth interval and suggested time (< 130 ka BP), sediment core and seismic data from Sættem et al. (1992) identified a unit (unit E) with mainly bioturbated marine sediments overlain by layered glacimarine sediments. In other words, it correlates with our interpretation. U5a, U5b and U6 correspond to unit H of Larsen et al. (2003) in the Sørvestagneset 3D.

Correlation with the ice-proxy records and marine-isotope stages suggests, however, that unit U5 and U6 were deposited during the three latest ice sheet advances that occurred at MIS 2–4 (the Weichselian glaciations) (Elverhøi et al., 1998). These advances were relatively short-lived; they all

occurred between 110 ka and 20 ka (Huybers and Wunsch, 2005), which can explain some of the immature erosional surfaces and frequent gully-formation that characterize the units (Figs. 4–8). Such an interpretation of the seismic stratigraphy implies that unit U5 was deposited under two glacial-interstadial cycles at ~110–55 ka BP, whereas unit U6 exhibits the youngest debris flow deposits from the very last glacial maximum between 15 and 25 ka BP (Fig. 9). The ice record data indicate a less well-defined, fluctuating and warm glacial period with limited global ice extent (compared to other cycles) during the last 0.5 Ma. Warmer periods than older ice ages can explain the pervasiveness of gullies through unit U5b.

Summing up, we propose that the seismic dataset presented in this study provides a record of seven major glacial advances and retreats during deposition of the middle to late Pleistocene succession on the SW Barents Sea slope. We suggest a stratigraphic record of four glacialinterglacial cycles between ~440 and 130 ka BP (U1a, U1b, U3, and U4), comparable to the interpretation of Sættem et al. (1992) (Fig. 9). Units U1a, U1b, U3, U4, U5 and U6 likely represent GDF units deposited at different glacial maximums, U2 a gradual cooling period, U5a a longer interglacial period and U5b two short-lived Weichselian glacial cycles. Our interpretations match the regional unit divisions by Sættem et al. (1992) followed by Laberg and Vorren (1996) and Svendsen et al. (2004).

Previous investigations by Vorren et al. (1990), Larsen et al. (2003) and King et al. (2014) indicate a dominance of glacigenic debris flow (GDFs) reflecting the depositional environment from the middle to the late Pleistocene along the entire SW Barents Sea. Reconstructions show that the Barents Sea margin experienced polar ice-front conditions during the middle-late Pleistocene which is suggested to explain the absence of channelized meltwater flow (Laberg et al., 2010). We provide new evidence that gullies and channels indicating periods of ice sheet melting and meltwater runoff existed throughout the middle-late Pleistocene succession, and thus new insight into the stratigraphic evolution of the Bear Island TMF and comparable continental margins dominated by GDFs around the world.

5. Evolution of slope, gullies, channels and bottom environment the last 0.5 Ma

Along the studied part the SW Barents Sea continental slope, the seafloor is dominated by shallow braided channels, only present on the upper continental slope (King et al., 2014). Down-slope gravity processes and ice-rafted debris flows usually become less common as the ice retreats from the shelf edge (Dowdeswell et al., 2016). Therefore, glacial debris flows are typically exposed on the upper slope, while a transition to glaciomarine mud occurs downslope where gravity flows become less erosive. In our seismic data, we observe gentle surfaces without distinct channels along

385 the deeper horizon H1 and H2. H3 shows underdeveloped gullies, while H4 small, narrow gullies and
386 H5 large slope gullies (Fig. 4).

387 Even within such a small 24 km2 area imaged by our HighRes 3D seismic cube (Fig. 1), the level,
388 pattern, and direction of erosional and depositional changes through time can be studied. Different
389 horizon and unit characteristics might be explained by other processes than icesheet dynamics.

390 Within the middle to late Pleistocene succession, we observe a gradual change of the dip-
391 orientation of the paleo slope from ENE-WSW along the deeper horizons R1 to H3 to NE-SW along
392 the shallower horizons H4-H5 (Figs. 2 and 10). Similar trends are found for downslope sediment
393 transport directions, even though occasionally skewed by 15–20 degrees (H3, H5) (Fig. 10). We
394 suggest that the changes might be caused by (1) a slight skew in ice-flow direction through time, or
395 (2) a higher sediment flux from the north, i.e., from the core of the Bear Island TMF that built out the
396 margin towards the south in this area. We propose that during deposition of unit U1 to U6, the
397 southern flank of the TMF consequently rotated south-westwards with increasing sediment input.

398 To test the possibility of the first scenario, we compared orientations of former ice-flows in the
399 Sørvestagneset 3D seismic area on the shelf further east (Larsen et al., 2003) with slope orientations
400 in our study area. We found a correlation between their results and ours, which is WSW directed ice-
401 stream lineations along R1 defining the base of the Middle-Late Pleistocene succession and a
402 transition to SW directed ice lineations of the seafloor (Fig. 10). The results likely indicate a change of
403 marginal ice-flow directions due to progradation and build out of the Bear Island TMF trough this
404 time.

405 A prograding shelf margin might have triggered more pervasive channel formation. From the 2D
406 seismic data, we observe at least 30 km of shelf-break progradation from exposure of H1 (~340–325
407 ka BP) to today's seafloor (Fig. 2). Taking an average continental slope dip of 2° and a sound-velocity
408 in water of 1500 m/s, horizons H3 and H1 (Fig. 6) were deposited in water depths of c. 680 m and
409 880 m, respectively (assuming a similar sea level during interglacials as today). This supposedly large
410 span in interglacial and glacial seafloor depth will significantly alter the depositional environment.

411 Sandwaves are extensive along the SW Barents Sea slope and occur on top of the glacial debris
412 flows and channels in the southern and northern areas in water depths from ~460 to 800 m at a
413 slope orientation ~NW-SE (King et al., 2014). Here, bottom currents reach speeds of > 0.75 m/s
414 (Skarðhamar et al., 2015). Similar conditions are expected to have occurred during previous
415 comparable interglacial periods. However, there are no signs of sandwaves along earlier interglacial
416 surfaces imaged by the 3D seismic cube.

The lack of sandwaves could be related to different water-depths or/ and slope orientations and thus different intensity of bottom-currents. The northern part of our study area shows a change in slope orientation from ENE-WSW to NW-SE. The depth interval for sandwave field build up shows clearly a preferred range (in our area between 550 and 660 m water depth) where both sediment supply and bottom current speeds are high enough. Alternatively, as all interpreted horizons are unconformities, along-slope and downslope processes may have eroded sandwave fields deposited during earlier interglacials.

6. Summary and conclusions

This study provides new insights into the stratigraphic evolution of a continental margin dominated by GDFs. By use of a small, but highresolution, P-Cable 3D seismic cube on the southern flank of the Bear Island Trough Mouth Fan (at the upper continental slope of the SW Barents Sea) we spatially reconcile multiple generations of glacigenic debris-flows. We identify seven distinct sediment units separated by characteristic seismic horizons suggested to represent seven glacial–interglacial/interstadial cycles deposited since MIS 12. Frequent shelf-edge ice sheet advances and retreats and periods of intense meltwater supply likely trigged massive debris flow deposition alternating with channel and gully formation. During interglacials (or interstadials), seismically well-defined surfaces developed indicating erosion and time hiatuses. Paleo-slope orientations indicate variations in marginal ice-flow direction related to delta-like progradation of the trough mouth fan. In contrast to previous observations, this study shows the presence of abundant gullies and channels throughout the middle to late Pleistocene succession indicating the influence of frequent episodes of meltwater discharge. The study contributes to a better understanding of the depositional environment on continental margins dominated by GDFs and demonstrates the usefulness of high-resolution seismic, such as the P-Cable system, for resolving the details of paleoslope environments.

Acknowledgments

This research was supported by MAREANO (www.mareano.no) and the Norwegian Deepwater Programme – Seabed Project (http://epim. no/npd/) to which we express our thanks. The research is also a part of the Centre for Arctic Gas Hydrate, Environment, and Climate and was supported by the Research Council of Norway through its Centres of Excellence funding scheme grant no. 223259. The first author spent a considerable time of her PhD for this work, which is funded by VISTA – a basic research program in collaboration between The Norwegian Academy of Science and Letters, and

Statoil that funds the PhD project. We are thankful to Schlumberger for providing their Petrel Interpretation and Visualization software. As a part of MAREANO, we thank the Norwegian Mapping Authority and the Norwegian Defense Research Establishment (FFI) for acquiring the multibeam echosounder bathymetry used in Fig. 1. We thank Monica Winsborrow for improving the lanuage, and also David J. Piper and another anonymous reviewer for constructive comments and ideas to improve the manuscript.

Appendix A.

Supplementary data Supplementary data to this article can be found online at https:// doi.org/10.1016/j.margeo.2018.05.006.

References

Andreassen, K., Ødegaard, C.M., Rafaelsen, B., 2007. Imprints of former ice streams, imaged and interpreted using industry three-dimensional seismic data from the south-western Barents Sea. Geol. Soc. Lond., Spec. Publ. 277, 151–169.

Bellec, V.K., Rise, L., Bøe, R., Dowdeswell, J.A., 2016. Glacially related gullies on the upper continental slope, SW Barents Sea margin. Geol. Soc. Lond. Mem. 46, 381–382.

Bøe, R., Skarðhamar, J., Rise, L., Dolan, M.F.J., Bellec, V.K., Winsborrow, M., Skagseth, Ø., Knies, J., King, E.L., Walderhaug, O., Chand, S., Buenz, S., Mienert, J., 2015. Sandwaves and sand transport on the Barents Sea continental slope offshore northern Norway. Mar. Pet. Geol. 60, 34–53.

Brown, A.R., Brown, A.R., Brown, A.R., Géophysicien, E.-U., Brown, A.R., 1996. Interpretation of Three-dimensional Seismic Data.

Bryn, P., Berg, K., Stoker, M.S., Haflidason, H., Solheim, A., 2005. Contourites and their relevance for mass wasting along the Mid-Norwegian Margin. Mar. Pet. Geol. 22, 85–96.

Buhl-Mortensen, L., Hodnesdal, H., Thorsnes, T., 2015. The Norwegian Sea Floor. 2015 MAREANO (Book). Butt, F.A., Elverhøi, A., Solheim, A., Forsberg, C.F., 2000. Deciphering Late Cenozoic development of the western Svalbard Margin from ODP site 986 results. Mar. Geol. 169, 373–390. Christensen, N.I., Mooney, W.D., 1995. Seismic velocity structure and composition of the continental crust: a global view. J. Geophys. Res. Solid Earth 100, 9761–9788. Culick, F., 1987. A note on Rayleigh's criterion. Combust. Sci. Technol. 56, 159–166.

Dowdeswell, J.A., Canals, M., Jakobsson, M., Todd, B.J., Dowdeswell, E.K., Hogan, K., 2016. Atlas of submarine glacial landforms: modern, Quaternary and ancient. Geol. Soc. Lond. 46 (1), 3–14. Elverhøi, A., Hooke, R.L., Solheim, A., 1998. Late Cenozoic erosion and sediment yield from the

480 Svalbard–Barents Sea region: implications for understanding erosion of glacierized basins. Quat. Sci.
481 Rev. 17, 209–241.

482 Faleide, J.I., Solheim, A., Fiedler, A., Hjelstuen, B.O., Andersen, E.S., Vanneste, K., 1996. Late Cenozoic
483 evolution of the western Barents Sea-Svalbard continental margin. Glob. Planet. Chang. 12, 53–74.
484 Fiedler, A., Faleide, J.I., 1996. Cenozoic sedimentation along the southwestern Barents Sea margin in
485 relation to uplift and erosion of the shelf. Glob. Planet. Chang. 12, 75–93.

486 Gales, J.A., Forwick, M., Laberg, J.S., Vorren, T.O., Larter, R.D., Graham, A.G.C., Baeten, N.J.,
487 Amundsen, H.B., 2013. Arctic and Antarctic submarine gullies—a comparison of high latitude
488 continental margins. Geomorphology 201, 449–461. Huybers, P., Wunsch, C., 2005. Obliquity pacing
489 of the late Pleistocene glacial terminations. Nature 434, 491–494.

490 Jakobsson, M., Andreassen, K., Bjarnadóttir, L.R., Dove, D., Dowdeswell, J.A., England, J.H., Funder, S.,
491 Hogan, K., Ingólfsson, Ó., Jennings, A., Krog Larsen, N., Kirchner, N., Landvik, J.Y., Mayer, L.,
492 Mikkelsen, N., Möller, P., Niessen, F., Nilsson, J., O'Regan, M., Polyak, L., Nørgaard-Pedersen, N.,
493 Stein, R., 2014. Arctic Ocean glacial history. Quat. Sci. Rev. 92, 40–67. Kenyon, N.H., 1986. Evidence
494 from bedforms for a strong poleward current along the upper continental slope of northwest Europe.
495 Mar. Geol. 72, 187–198.

496 Kenyon, N.H., 1987. Mass-wasting features on the continental slope of northwest Europe. Mar. Geol.
497 74, 57–77. King, E.L., Bøe, R., Bellec, V.K., Rise, L., Skarðhamar, J., Ferré, B., Dolan, M.F.J., 2014.
498 Contour current driven continental slope-situated sandwaves with effects from secondary current
499 processes on the Barents Sea margin offshore Norway. Mar. Geol. 353, 108–127.

500 Laberg, J.S., Vorren, T.O., 1995. Late Weichselian submarine debris flow deposits on the Bear Island
501 trough mouth fan. Mar. Geol. 127, 45–72.

502 Laberg, J.S., Vorren, T.O., 1996. The middle and late Pleistocence evolution and the Bear Island
503 trough mouth fan. Glob. Planet. Chang. 12, 309–330.

504 Laberg, J.S., Andreassen, K., Knies, J., Vorren, T.O., Winsborrow, M., 2010. Late Pliocene–Pleistocene
505 development of the Barents Sea ice sheet. Geology 38, 107–110.

506 Laberg, J.S., Andreassen, K., Vorren, T.O., 2012. Late Cenozoic erosion of the high-latitude
507 southwestern Barents Sea shelf revisited. Geol. Soc. Am. Bull. 124, 77–88.

508 Larsen, E., Andreassen, K., Nilssen, L.C., Raunholm, S., 2003. The prospectivity of the Barents Sea: ice
509 ages, erosion and tilting of traps. NGU-rapport 2003, 102 (60 p).

Lowe, A.L., Anderson, J.B., 2003. Evidence for abundant subglacial meltwater beneath the paleo-ice sheet in Pine Island bay, Antarctica. J. Glaciol. 49, 125–138.

Petersen, C.J., Bünz, S., Hustoft, S., Mienert, J., Klaeschen, D., 2010. High-resolution Pcable 3D seismic imaging of gas chimney structures in gas hydrated sediments of an Arctic sediment drift. Mar. Pet. Geol. 27, 1981–1994.

Piper, D.J., 1988. DNAG# 3. Glaciomarine sedimentation on the continental slope off eastern Canada. Geosci. Can. 15. Piper, D.J., 2005. Late Cenozoic evolution of the continental margin of eastern Canada. Nor. J. Geol. 85.

Posamentier, H.W., Kolla, V., 2003. Seismic geomorphology and stratigraphy of depositional elements in deep-water settings. J. Sediment. Res. 73, 367–388.

Poulain, P.M., Warn-Varnas, A., Niiler, P.P., 1996. Near-surface circulation of the Nordic seas as measured by Lagrangian drifters. J. Geophys. Res. Oceans 101, 18237–18258.

Reimchen, A.P., Hubbard, S.M., Stright, L., Romans, B.W., 2016. Using sea-floor morphometrics to constrain stratigraphic models of sinuous submarine channel systems. Mar. Pet. Geol. 77, 92–115.
Ryseth, A., Harald, J., Augustson, Charnock, M., Haugerud, O., Stig-Morten, K., Midbøe, Peter S., Opsal, J.G., Sundsbø, G., 2003. Cenozoic stratigraphy and evolution of the Sørvestsnaget Basin, southwestern Barents Sea. Nor. J. Geol. 83, 107–130.

Sættem, J., Poole, D.A.R., Ellingsen, L., Sejrup, H.P., 1992. Glacial geology of outer Bjørnøyrenna, southwestern Barents Sea. Mar. Geol. 103, 15–51.

Sættem, J., Bugge, T., Fanavoll, S., Goll, R.M., Mørk, A., Mørk, M.B.E., Smelror, M., Verdenius, J.G., 1994. Cenozoic margin development and erosion of the Barents Sea: core evidence from southwest of Bjørnøya. Mar. Geol. 118, 257–281.

Sejrup, H.P., Hjelstuen, B.O., Torbjørn Dahlgren, K.I., Haflidason, H., Kuijpers, A., Nygård, A., Praeg, D., Stoker, M.S., Vorren, T.O., 2005. Pleistocene glacial history of the NW European continental margin. Mar. Pet. Geol. 22, 1111–1129.

Skarðhamar, J., Skagseth, Ø., Albretsen, J., 2015. Diurnal tides on the Barents Sea continental slope. Deep-Sea Res. I Oceanogr. Res. Pap. 97, 40–51.

Solheim, A., Andersen, E.S., Elverhøi, A., Fiedler, A., 1996. Late Cenozoic depositional history of the western Svalbard continental shelf, controlled by subsidence and climate. Glob. Planet. Chang. 12, 135–148.

Spinelli, G.A., Field, M.E., 2001. Evolution of continental slope gullies on the northern California margin. J. Sediment. Res. 71, 237–245.

Stravers, J.A., Powell, R.D., 1997. Glacial debris flow deposits on the Baffin Island shelf: seismic facies architecture of till-tongue-like deposits. Mar. Geol. 143, 151–168.

Svendsen, J.I., Alexanderson, H., Astakhov, V.I., Demidov, I., Dowdeswell, J.A., Funder, S., Gataullin, V., Henriksen, M., Hjort, C., Houmark-Nielsen, M., Hubberten, H.W., Ingólfsson, Ó., Jakobsson, M., Kjær, K.H., Larsen, E., Lokrantz, H., Lunkka, J.P., Lysså, A., Mangerud, J., Matiouchkov, A., Murray, A., Möller, P., Niessen, F., Nikolskaya, O., Polyak, L., Saarnisto, M., Siegert, C., Siegert, M.J., Spielhagen, R.F., Stein, R., 2004. Late Quaternary ice sheet history of northern Eurasia. Quat. Sci. Rev. 23, 1229–1271.

Syvitski, J.P., 1991. Towards an understanding of sediment deposition on glaciated continental shelves. Cont. Shelf Res. 11, 897–937.

Twichell, D.C., Roberts, D.G., 1982. Morphology, distribution, and development of submarine canyons on the United States Atlantic continental slope between Hudson arid Baltimore canyons. Geology 10, 408–412.

Vorren, T.O., Laberg, J.S., 1997. Trough mouth fans — palaeoclimate and ice-sheet monitors. Quat. Sci. Rev. 16, 865–881.

Vorren, T.O., Lebesbye, E., Andreassen, K., Larsen, K.B., 1989. Glacigenic sediments on a passive continental margin as exemplified by the Barents Sea. Mar. Geol. 85, 251–272.

Vorren, T.O., Lebesbye, E., Larsen, K.B., 1990. Geometry and genesis of the glacigenic sediments in the southern Barents Sea. Geol. Soc. Lond., Spec. Publ. 53, 269–288.

Vorren, T., Laberg, J.S., Blaume, F., Dowdeswell, J.A., Kenyon, N.H., Mienert, J., Rumohr, J.A.N., Werner, F., 1998. The Norwegian–Greenland Sea continental margins: Morphology and late quaternary sedimentary processes and environment. Quat. Sci. Rev. 17, 273–302

Figure captions

Fig. 1. Study Area. (A) Shaded relief map of the South Western Barents Sea with Last Glacial Maximum (LGM) and main ice stream directions indicated. The red square highlights the study area. The white square marks the location of the previously investigated Sørvestagneset 3D cube used for seismic correlation. (B) Bathymetry in the study area (red square in A) showing sandwaves, slope-channels, and glacigenic debris flows. Outline of the 3D seismic survey area is shown. (For interpretation of the references to colour in this figure legend, the reader is referred to the web version of this article.)

Fig. 2. Seismic correlation line from Sørvestagneset 3D (outer shelf) via 2D seismic lines (NH9702 survey) to study area (SandWaveNorth 3D) using Larsen et al. (2003) as a reference. The seismic boundaries between Larsen et al. (2003) units E to H can be traced from the Sørvestagneset 3D cube via 2D seismic lines. In this study, we identify six units named U1–U6, and six horizons; R1, and H1 to H5 within the regional unit GIII. Unit E and partly unit F appear to correlate with our unit U1–U3, unit G with our unit U4, and unit H with units U5 and U6. The panel in the lower left corner indicates the location of the correlation line.

Fig. 3. Left panel shows inline 52 and x-line 1590 with units and horizons interpreted in this study. Lower left inset A (location is shown in left panel) is a close-up of inline 92, with channels occurring along H5 and H4 and debris flows within units U5 and U6. Here, underlying reflectors are clearly cut at the H5 channel walls. The right panel shows interpreted surfaces with typical features; horizon H5 (large channels), H4 (narrow channels), H3 (shallow channels), Intra U2 (a network of indistinct channels) and H1 (smooth surface) and indicated slope-direction based on contour lines.

Fig. 4. Seismic inline 201 and xline 342 without and with seismic interpretation. Within units, mounded to straight seismic reflectors appear and the seismic varies from semi-transparent (U1, between sub-parallel reflectors within U2–U6) to more chaotic (mainly U5 and U6). Narrow and straight to slightly sinuous V-shaped reflectors occur within U4 and U3. Along H4, such reflectors are most likely small gullies, identified by higher amplitudes along thalwegs/gully bases. R1 is more undulating than the other main horizons that have an overall similar slope gradient. More continuous reflectors occur in the middle of U1 (blue stippled line) and U5 (yellow stippled line cut by gullies). (For interpretation of the references to colour in this figure legend, the reader is referred to the web version of this article.)

Fig. 5. RMS-amplitude attribute surface (± 5m above the surface) of horizon H2 identifies several straight, high-amplitude bands, here interpreted to reflect the position of the bases/thalweg of seismically indistinct channels within unit U3. The location of the line is shown in Fig. 4.

602 Fig. 6. Root Mean Square (RMS) amplitude attribute map indicate high reflection amplitudes in gully
603 thalwegs/bases at (A) horizon H5, (B) within unit U5 with a minor shift (± 10 m) to incorporate H4
604 and H5 and (C) along horizon H4. (D) Show RMS amplitude of U4 (minus 20 ms from H4). Zoom-in
605 profile (E) and Fig. 4 show the stratigraphic location.

606 Fig. 7. Example of reflector "intra U5" within unit U5 that is interpreted within a debris flow-
607 dominated interval along two erosional flanks about 3 km apart. Approximate location is shown in
608 Fig. 4.

609 Fig. 8. (A) and (B) show that unit U6 represents channel fill with a semi-transparent to chaotic seismic
610 signature and that it is interbedded by 1–2 more continuous horizons. (C) Snapshot of the overlying
611 seafloor with migrating sandwaves.

612 Fig. 9. Composite diagram showing A) global temperature and ice volume data from oxygen isotope
613 proxy and marine isotope stages (MIS) from the EPICA Dome C ice cores in Antarctica. B) Suggested
614 glaciation curve for the Western Barents Sea from Svendsen et al. (2004) and Larsen et al. (2003). C)
615 Correlation table of seismic units and horizons from the studies discussed including this study.

616 Fig. 10. Contour lines (30 m) and gully/channel orientation of surfaces R1 to H5. To the lower left, we
617 show the average contour trend and dip direction. In the table to the right, dip direction and
618 gully/channel orientations are compared with the direction of former ice-flows on the outer shelf at
619 Sørvestagneset 3D (Larsen et al., 2003). The figure indicates that the dip of the slope (and therefore
620 also slope orientation) has changed slightly from WSW-ENE to SW-NE during deposition of GIII.

621

622

623

624

625

626

627

628

629

630

631 **Figures**

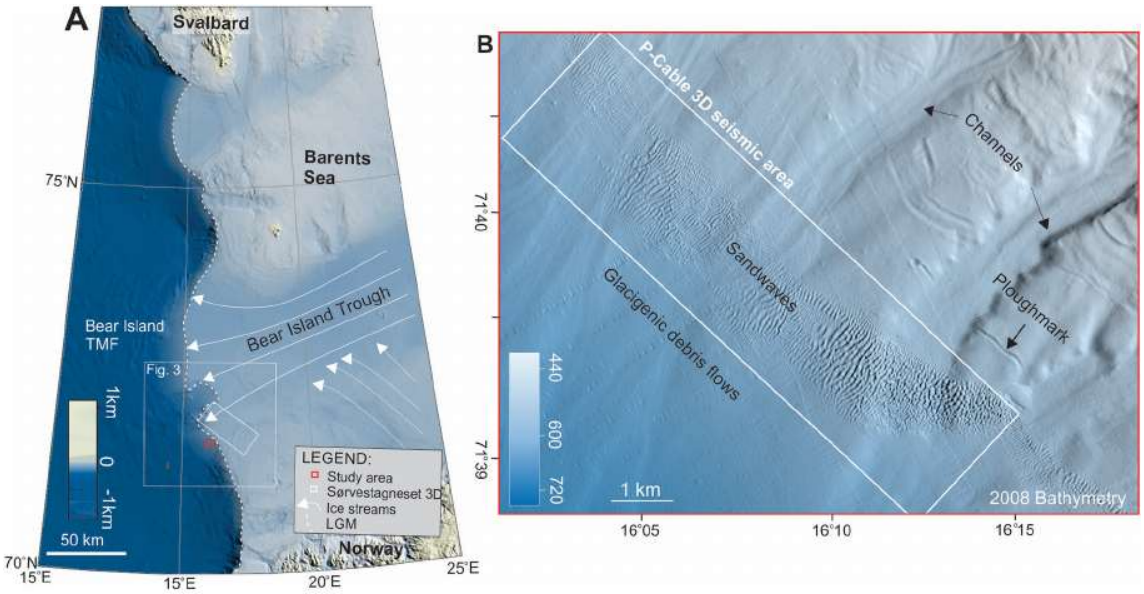

632

633 Fig. 1. Study Area. (A) Shaded relief map of the South Western Barents Sea with Last Glacial
634 Maximum (LGM) and main ice stream directions indicated. The red square highlights the study area.
635 The white square marks the location of the previously investigated Sørvestagneset 3D cube used for
636 seismic correlation. (B) Bathymetry in the study area (red square in A) showing sandwaves, slope-
637 channels, and glacigenic debris flows. Outline of the 3D seismic survey area is shown. (For
638 interpretation of the references to colour in this figure legend, the reader is referred to the web
639 version of this article.)

640

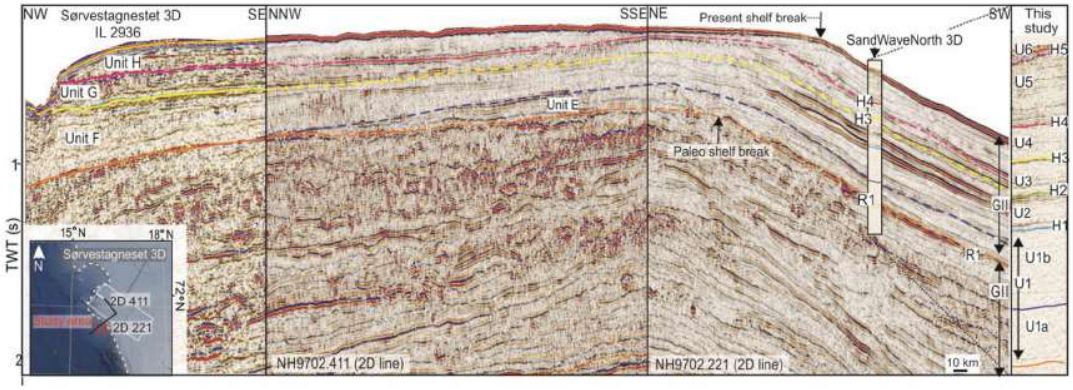

641

642 Fig. 2. Seismic correlation line from Sørvestagneset 3D (outer shelf) via 2D seismic lines (NH9702
643 survey) to study area (SandWaveNorth 3D) using Larsen et al. (2003) as a reference. The seismic
644 boundaries between Larsen et al. (2003) units E to H can be traced from the Sørvestagneset 3D cube

via 2D seismic lines. In this study, we identify six units named U1–U6, and six horizons; R1, and H1 to H5 within the regional unit GIII. Unit E and partly unit F appear to correlate with our unit U1–U3, unit G with our unit U4, and unit H with units U5 and U6. The panel in the lower left corner indicates the location of the correlation line.

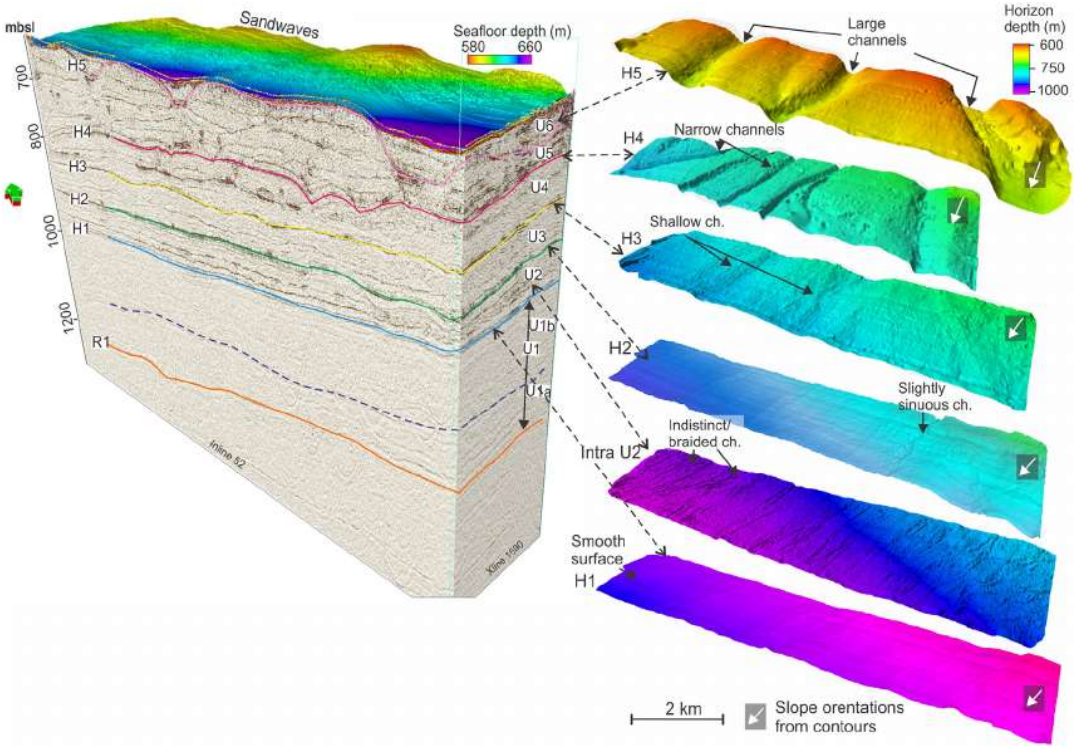

Fig. 3. Left panel shows inline 52 and x-line 1590 with units and horizons interpreted in this study. Lower left inset A (location is shown in left panel) is a close-up of inline 92, with channels occurring along H5 and H4 and debris flows within units U5 and U6. Here, underlying reflectors are clearly cut at the H5 channel walls. The right panel shows interpreted surfaces with typical features; horizon H5 (large channels), H4 (narrow channels), H3 (shallow channels), Intra U2 (a network of indistinct channels) and H1 (smooth surface) and indicated slope-direction based on contour lines.

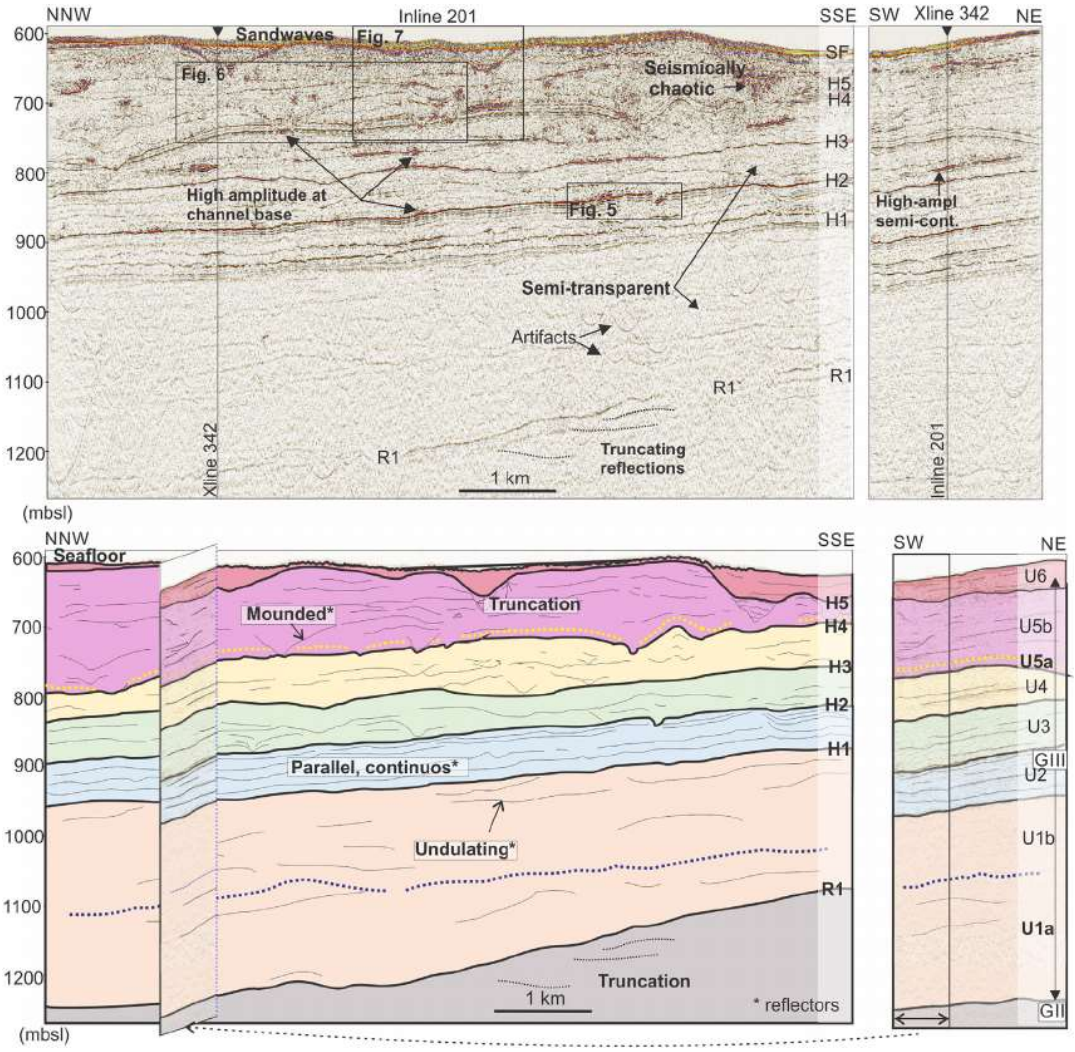

Fig. 4. Seismic inline 201 and xline 342 without and with seismic interpretation. Within units, mounded to straight seismic reflectors appear and the seismic varies from semi-transparent (U1, between sub-parallel reflectors within U2–U6) to more chaotic (mainly U5 and U6). Narrow and straight to slightly sinuous V-shaped reflectors occur within U4 and U3. Along H4, such reflectors are most likely small gullies, identified by higher amplitudes along thalwegs/gully bases. R1 is more undulating than the other main horizons that have an overall similar slope gradient. More continuous reflectors occur in the middle of U1 (blue stippled line) and U5 (yellow stippled line cut by gullies). (For interpretation of the references to colour in this figure legend, the reader is referred to the web version of this article.)

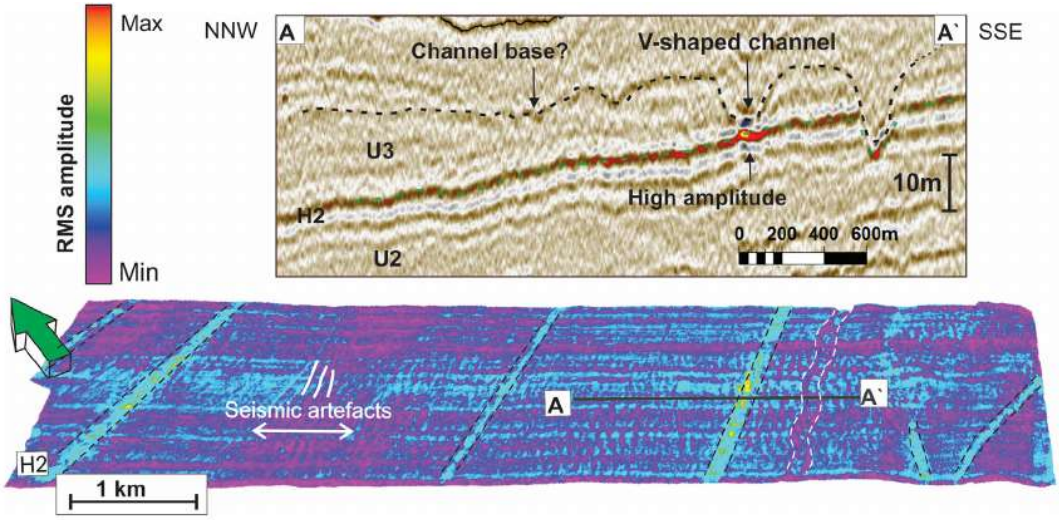

670

671 Fig. 5. RMS-amplitude attribute surface (± 5m above the surface) of horizon H2 identifies several
672 straight, high-amplitude bands, here interpreted to reflect the position of the bases/thalweg of
673 seismically indistinct channels within unit U3. The location of the line is shown in Fig. 4.

674

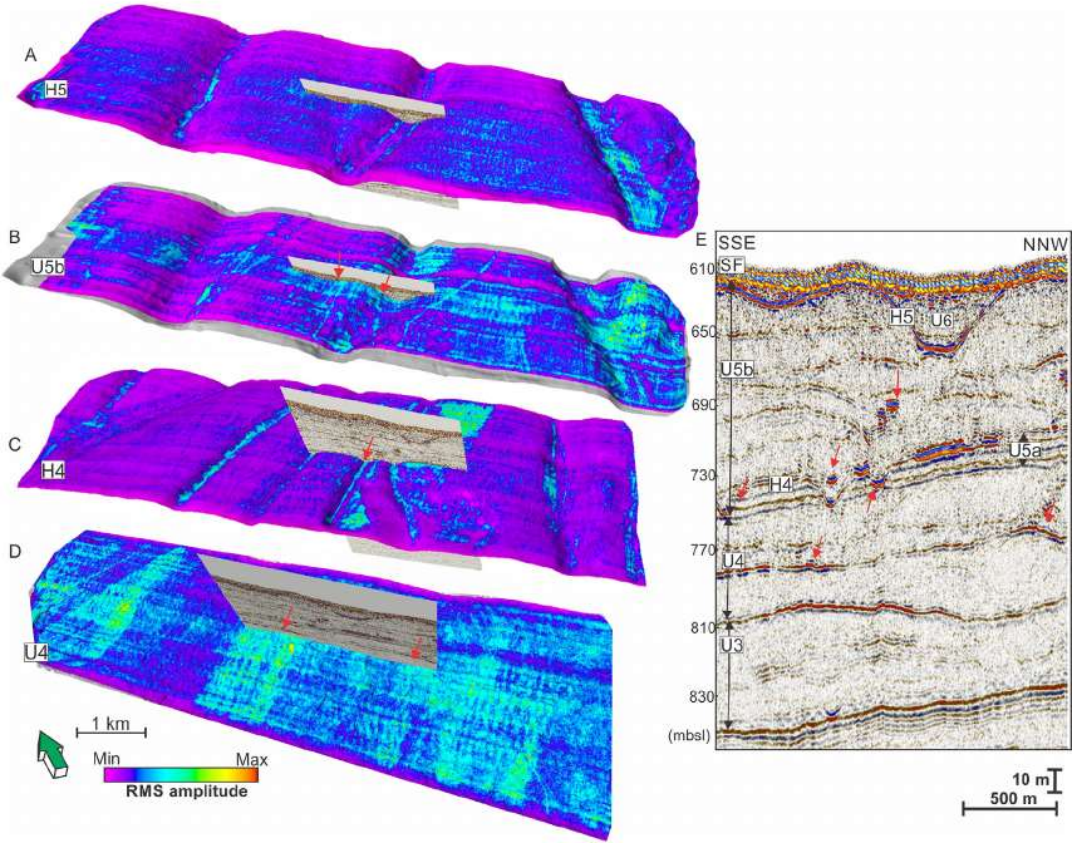

675

676

677 Fig. 6. Root Mean Square (RMS) amplitude attribute map indicate high reflection amplitudes in gully
678 thalwegs/bases at (A) horizon H5, (B) within unit U5 with a minor shift (± 10 m) to incorporate H4
679 and H5 and (C) along horizon H4. (D) Show RMS amplitude of U4 (minus 20 ms from H4). Zoom-in
680 profile (E) and Fig. 4 show the stratigraphic location.

681

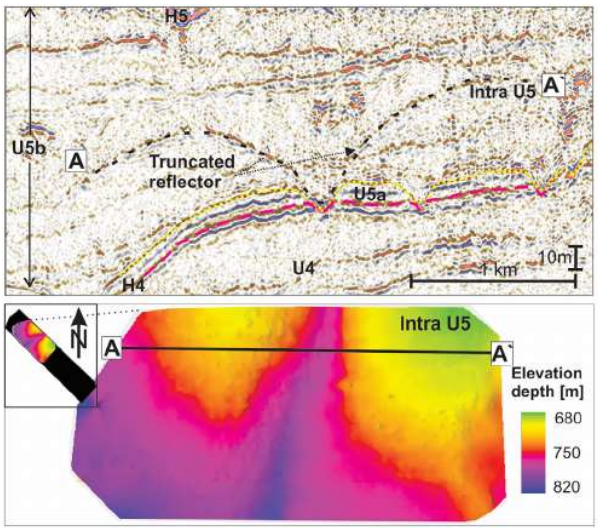

682

683 Fig. 7. Example of reflector “intra U5” within unit U5 that is interpreted within a debris flow-
684 dominated interval along two erosional flanks about 3 km apart. Approximate location is shown in
685 Fig. 4.

686

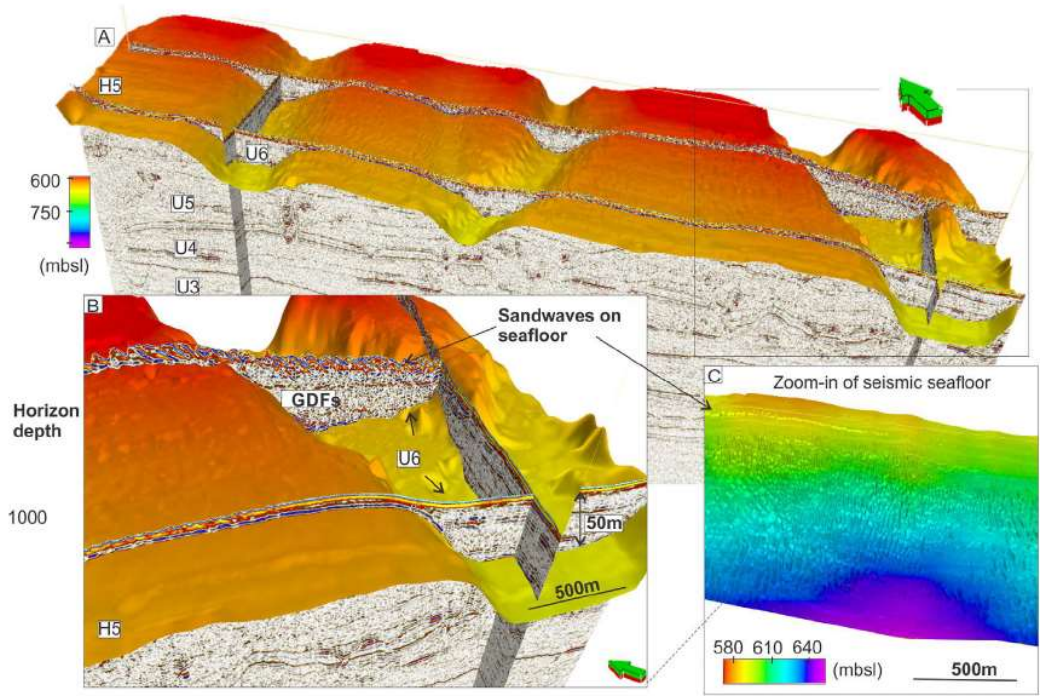

687

688 Fig. 8. (A) and (B) show that unit U6 represents channel fill with a semi-transparent to chaotic seismic
689 signature and that it is interbedded by 1–2 more continuous horizons. (C) Snapshot of the overlying
690 seafloor with migrating sandwaves.

691

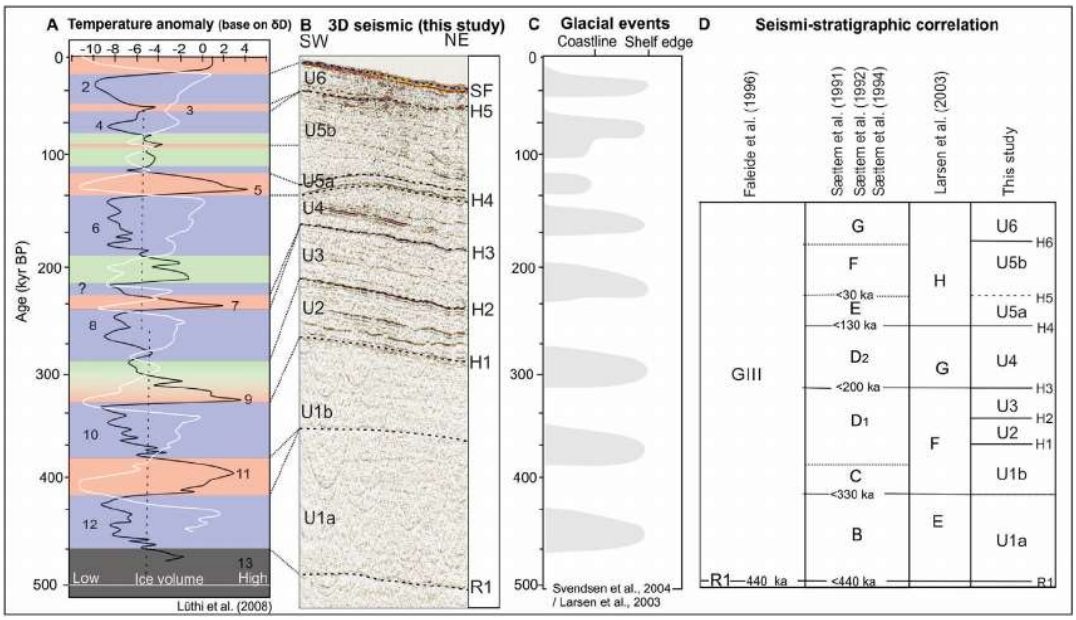

692

693 Fig. 9. Composite diagram showing A) global temperature and ice volume data from oxygen isotope
694 proxy and marine isotope stages (MIS) from the EPICA Dome C ice cores in Antarctica. B) Suggested

695 glaciation curve for the Western Barents Sea from Svendsen et al. (2004) and Larsen et al. (2003). C)
696 Correlation table of seismic units and horizons from the studies discussed including this study.

697 Fig. 10. Contour lines (30 m) and gully/channel orientation of surfaces R1 to H5. To the lower left, we
698 show the average contour trend and dip direction. In the table to the right, dip direction and
699 gully/channel orientations are compared with the direction of former ice-flows on the outer shelf at
700 Sørvestagneset 3D (Larsen et al., 2003). The figure indicates that the dip of the slope (and therefore
701 also slope orientation) has changed slightly from WSW-ENE to SW-NE during deposition of GIII.

702